Journal of Hazardous Materials 403 (2021) 123547

Contents lists available at ScienceDirect

Journal of Hazardous Materials

journal homepage: www.elsevier.com/locate/jhazmat

Multifunctional CNTs-PAA/MIL101(Fe)@Pt Composite Membrane for High-throughput Oily Wastewater Remediation

Chaohui Liu [a,1], Junyuan Xia [b,1], Jincui Gu [b,c,*], Wenqin Wang [d], Qingquan Liu [e], Luke Yan [a,**], Tao Chen [a,b,c,**]

[a] Polymer Materials & Engineering Department, School of Materials Science & Engineering, Chang' an University, Xi'an, 710064, China
[b] Key Laboratory of Marine Materials and Related Technologies, Zhejiang Key Laboratory of Marine Materials and Protective Technologies, Ningbo Institute of Material Technology and Engineering, Chinese Academy of Science, Ningbo 315201, China
[c] University of Chinese Academy of Science, Beijing 100049, China
[d] Faculty of Materials Science and Chemical Engineering, Ningbo University, 818 Fenghua Road, Ningbo 315211, China
[e] Institute of Materials Science and Engineering, Hunan University of Science and Technology, Xiangtan 411201, China

ARTICLE INFO

Editor: Danmeng Shuai

Keywords:
CNTs-PAA membrane
MIL101(Fe)@Pt NPs
Synergistic separation
Versatility
Stability

ABSTRACT

A surge of effort has been devoted to establishing super-wetting membranes with versatility for oily waste water purification. However, persistent challenge remains the lower separation flux. Moreover, the majorities of catalysts are only adsorbed on the surface and easily fall off after multiple cyclic separations. In this work, an effective strategy has been taken to construct a composite membrane consisting of polyacrylic acid functionalized carbon nanotubes (CNTs-PAA) and MIL101(Fe)@platinum nanoparticles (MIL101(Fe)@Pt NPs). The obtained CNTs-PAA/MIL101(Fe)@Pt composite membrane can achieve degradation of dye molecules and at the same time effective separation of oil-in-water emulsions. The separation throughput of this composite membrane can reach up to 11000 L m^{-2} h^{-1} bar^{-1}, which has exceeded most of the previous reported multifunctional separation membranes. Furthermore, this composite membrane has presented stable mechanical property and excellent anti-corrosion ability. This work gives comprehensive consideration to excellent separation performance, versatility and stability, which could have potential applications in practical oily wastewater treatment.

1. Introduction

The purification of oily wastewater has become a significant topic owing to the frequent oil spill incidents and the ever-increasing demand for environmental protection (Wang et al., 2015a; Ge et al., 2016; Li et al., 2018a; Zhang et al., 2018a). Inspired by nature, super-wetting materials have become the most promising candidates to address these problems since Feng and co-workers have firstly designed a superhydrophobic mesh for oil/water mixture separation (Feng et al., 2004). Afterwards, various materials are merged in endlessly. Generally speaking, these materials can be categorized into four groups, superhydrophobic/superoleophilic materials, such as particles (Song et al., 2018; Zhu et al., 2014; Wang et al., 2015b; Duan et al., 2015), sponges/foam (Wang et al., 2018a; Wang et al., 2019), fabrics (Wang et al., 2020a; Zhang et al., 2018b), membranes (Cao et al., 2019; Wang et al., 2020b) and meshes (Wang et al., 2015c; Li et al., 2016a; Zhang et al., 2019a), superhydrophilic/superoleophobic materials (Gao et al., 2015; Liu et al., 2018; Liu et al., 2015), Janus materials (Hu et al., 2015; Yang et al., 2019; An et al., 2018), and smart materials with switchable wettability through adjusting external stimuli (Liu et al., 2017; Fu et al., 2017; Dutta et al., 2017). Membrane with special surface wettability is considered to be one of the most potential materials for oily wastewater purification on large-scale due to its convenient separation equipment and low-energy consumption (Chen et al., 2017). Numerous separation membranes, such as poly () membrane (Wei et al., 2018), polytetrafluoroethylene membrane (Meng et al., 2018; Gupta et al., 2017) and polydimethylsiloxane membrane (Zhang et al., 2017), have been constantly designed. Carbon nanotubes (CNTs) have gained enormous

* Corresponding author at: Key Laboratory of Marine Materials and Related Technologies, Zhejiang Key Laboratory of Marine Materials and Protective Technologies, Ningbo Institute of Material Technology and Engineering, Chinese Academy of Science, Ningbo 315201, China.
** Corresponding authors at: Polymer Materials & Engineering Department, School of Materials Science & Engineering, Chang' an University, Xi'an, 710064, China.
E-mail addresses: gujincui@nimte.ac.cn (J. Gu), yanlk_79@hotmail.com (L. Yan), tao.chen@nimte.ac.cn (T. Chen).
[1] Chaohui Liu and Junyuan Xia contributed equally to this work.

https://doi.org/10.1016/j.jhazmat.2020.123547
Received 13 February 2020; Received in revised form 7 July 2020; Accepted 20 July 2020
Available online 11 August 2020

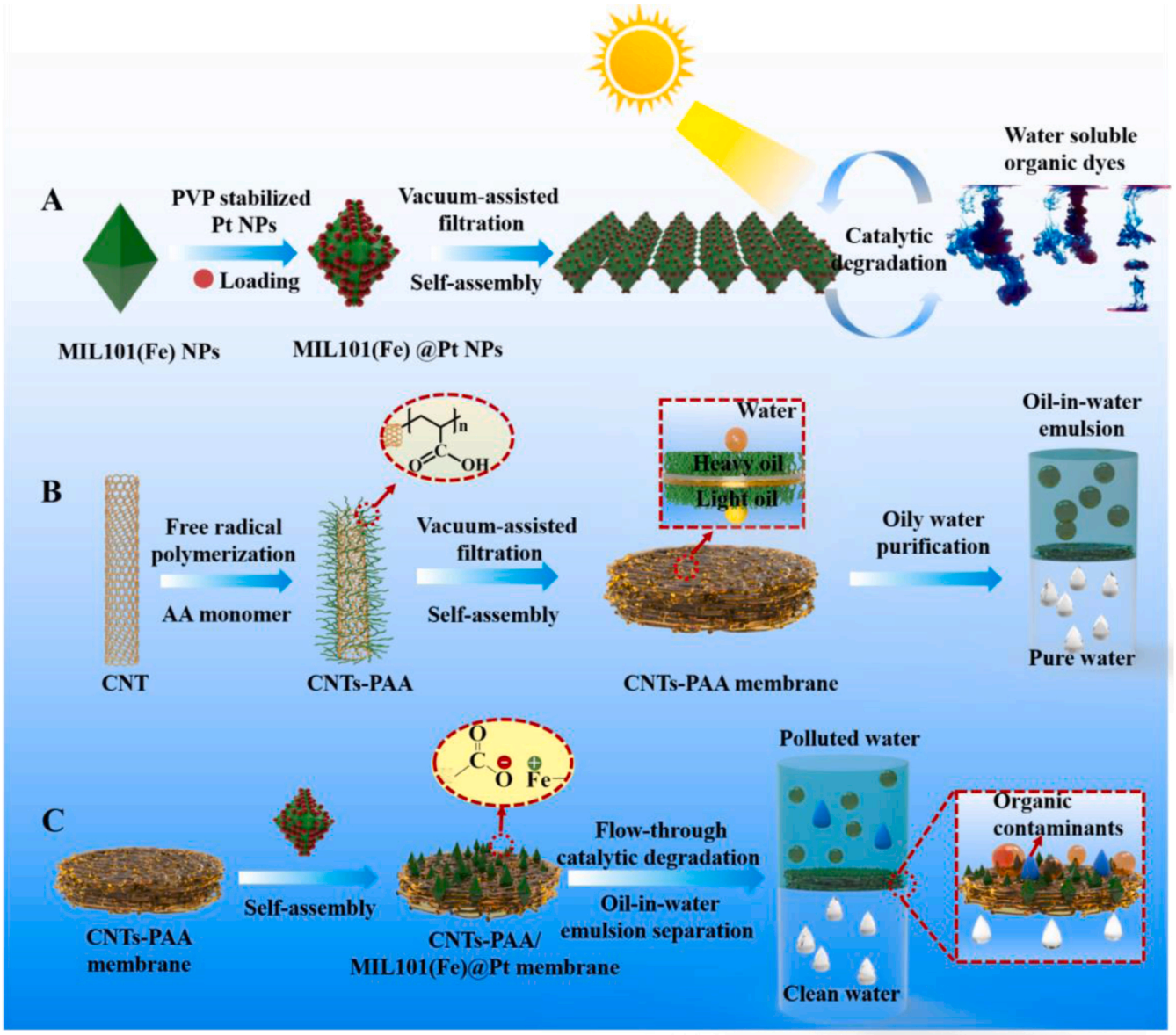

Fig. 1. Schematic illustration of the (A) construction of the MIL101(Fe)@Pt NPs for catalytic degradation of dyes pollutants, (B) the preparation process of superhydrophilic and underwater superoleophobic CNTs-PAA membrane for the separation of oil-in-water emulsion, and (C) the assemble of the CNTs-PAA/MIL101 (Fe)@Pt composite membrane for catalytic degradation of dye molecules and meanwhile separation of oil-in-water emulsion.

attentions owing to their remarkable physical and chemical properties, including high porosity and outstanding adsorption ability (Mi et al., 2017). In previous work, we have prepared a series of superhydrophobic polymer functionalized CNTs-based membranes with outstanding ability of separating water-in-oil emulsions (Gu et al., 2014a; Gu et al., 2015) and oil-in-water emulsions (Gu et al., 2014b). These membranes can separation oil/water emulsions at micro- or nano- scales but cannot remove soluble organic pollutants. Despite these progresses, the separated water phase is not suitable to discharge into the circulating water system even after several cycles of treatment. Therefore, a separation membrane material with versatility to effectively realize oily wastewater treatment is highly anticipated.

Catalytic degradation is regarded as the most practicable means to realize the elimination of water-soluble pollutions (Wang et al., 2016). Combining appropriate photocatalyst with super-wetting membranes can realize simultaneously the separation of oil-in-water emulsions and the decomposition of water-soluble organic contaminants (Li et al., 2016b). Liu et al. have prepared an Au-loaded porous (Au@ZIF-8@-PAN-TD) membrane through an electro-spinning and surface modification strategy (Zhang et al., 2019b). This composite membrane can achieve efficient emulsion separation and in situ catalytic degradation of 4-nitrophenol. Yan et al. have reported a PVDF/TA/β-FeOOH composite membrane, which has displayed good separation efficiency for dyes (~ 99.1 %) and high flux (~2106.2 L m^{-2} h^{-1} bar^{-1}) for oil-in-water emulsions (Xie et al., 2019). We have fabricated a series of CNT-based membrane through free radical polymerization and subsequently composite nanoparticles loaded (Zhang et al., 2016a; Yan et al., 2019). These membranes can purify oil-in-water emulsions with the flux as high as 3500 L m^{-2} h^{-1} bar^{-1} and catalytic degrade organic pollutants when the water permeated through the tortuous channels. Despite these progresses, the longer total distance has reduced the separation flux of these membranes (Shi et al., 2013). In addition, these nanoparticles are only adsorbed on the surface of these membranes and easily fall off after multiple cyclic separations. Therefore, it is urgent to construct membrane with short separation pathway and stable structure to endow it with excellent separation performance.

Metal-organic frameworks (MOFs), as an outstanding photo catalyst, have drawn increasing attention owing to their extensive potential in

water body restoration benefiting from their high specific surface areas, abundant metal/organic species, large pore volumes and extraordinary tenability of structures as well as compositions (Fang et al., 2019). Interesting studies have been attempted to employ MOFs for photocatalytic degradation of several organic dyes. Fe-based metal organic frameworks, such as MIL101(Fe), have generated numerous attentions due to their environmental friendliness, cost effective and photo responsive feature. Zhao et al. have obtained a composite with hetero-structure consisting of graphitic-carbon nitride (g-C_3N_4) and MIL101(Fe) (Gong et al., 2018). The g-C_3N_4/MIL101(Fe) composite can dramatically improve the photo catalytic degradation performance of g-C_3N_4 for bisphenol A attributed to the well-matched band structure between g-C_3N_4 and MIL01(Fe). Zhang et al. have constructed a MIL101 (Fe)@Pt@MIL101(Fe) composite with Pt NPs ebbing between the inner core and the outer shell of MIL101(Fe), resulting in stable catalysts for converting a range of α, β-unsaturated aldehydes with high efficiency and with significantly enhancing selectivity towards unsaturated alcohols (Zhang et al., 2016b).

Herein, we have fabricated a composite membrane consisting superhydrophilic/underwater superoleophobic polyacrylic acid functionalized carbon nanotubes (CNTs-PAA) and MIL101(Fe)@platinum nanoparticles (MIL101(Fe)@Pt NPs). The procedure for fabricating the CNTs-PAA/MIL101(Fe)@Pt composite membrane was schematically illustrated in Fig. 1. Firstly, MIL101(Fe) NPs with octahedral shape were encapsulated densely with Pt NPs (Fig. 1A). Secondly, hydrophilic PAA was grafted onto the surface of CNTs via free radical polymerization and afterward vacuum-assisted filtration to form a CNTs-PAA network membrane with superhydrophilicity/underwater superoleophobicity (Fig. 1B). Lastly, the MIL101(Fe)@Pt NPs were stably embedded into the CNTs-PAA membrane to form a catalytic layer via the electrostatic interaction (Wang et al., 2018b) (Fig. 1C). The obtained CNTs-PAA/MIL101(Fe)@Pt composite membrane can separate various oil-in-water emulsions with flux as high as 11,000 L m^{-2} h^{-1} bar^{-1} and realize catalytic degradation of dye pollutants. Furthermore, it has shown stable mechanical property and excellent anti-corrosion ability. In view of the outstanding comprehensive performance of this composite membrane, this work will widen the scope of CNTs-based membranes for wastewater purification.

2. Experimental

2.1. Materials

Carboxylated carbon nanotubes (CNTs, 5~20 μm length and 8~30 nm diameter, ~2.0 wt% −COOH) were obtained from Chengdu Organic Chemistry Co., Ltd. CNTs were rinsed thoroughly with anhydrous ethanol and consecutively dried in a stream of nitrogen before use. Acrylic acid (AA, purity>99 %) and benzoyl peroxide (BPO) were got from Sigma-Aldrich (Shanghai) Co., Ltd. Polyvinyl pyrrolidone (PVP, 55,000 g/mol) and iron chloride hexahydrate ($FeCl_36^{\bullet}H_2O$) were provided by Sigma-Aldrich (Shanghai) Co., Ltd. *N, N*-dimethylformamide (DMF) and 1, 4-benzenedicarboxylic acid (H_2BDC) were obtained from Aladdin (Shanghai) Co., Ltd. Chloroplatinic acid (H_2PtCl_6), sodium borohydride ($NaBH_4$) and methylene blue (MB, 98 wt%) were purchased from Alfa Aesar China (Tianjin) Co., Ltd. Other chemicals were provided by Sinopharm Chemical Reagent Co., Ltd. Polyvinylidene fluoride (PVDF) substance was got from Millipore Industrial & Lab Chemicals (aperture ~0.45 μm).

2.2. Preparation of CNTs-PAA composite membrane

CNTs-PAA composite membrane was fabricated according to the previous reported work (Zhang et al., 2016a, 2016b). 0.15 g of CNTs was dispersed into 100 mL of acetone. After stirring for 20 min at 25 °C, 3.5 g of AA was added under nitrogen environment and then stirring for 30 min. 0.065 g of BPO was added to initiate polymerization, which was maintained at 75 ℃ for 8 h. The PAA grafted CNTs (CNTs-PAA) membrane was got by filtration on the PVDF membrane and washed by ethyl acetate and deionized water alternately to remove residual AA. The CNTs-PAA membrane was dried at 40 ℃ for 20 h.

2.3. Preparation of Pt NPs

The Pt NPs was synthesized according to the literature (Yan et al., 2019). Firstly, 16.6 mg of PVP was dispersed in 45 mL of alcohol and then ultrasonic for 30 min at 35 °C. Secondly, 5 mL of H_2PtCl_6 was dropped into the above mixed solution slowly and stir for 10 min at 25 °C to form a homogeneous mixture. Lastly, the Pt NPs were obtained through reflux reaction for 3 h.

2.4. Preparation of MIL101 (Fe) NPs

The MIL101(Fe) was synthesized according to the literature (Zhang et al., 2016b). Firstly, 93.4 mg of $FeCl_36^{\bullet}H_2O$ and 57.5 mg of H_2BDC were added into 16 mL of DMF in succession and then stirred for 8 h at 160 °C. Secondly, the mixed solution was heated at 160 °C for 8 h under nitrogen atmosphere. Lastly, the sediment was collected by centrifugation at 8000 rpm for 10 min. The MIL101(Fe) NPs were rinsed with DMF for three times to remove unreacted ingredient in the solution. The achieved MIL101 (Fe) NPs were vacuum dried under 100 °C for 12 h.

2.5. Preparation of MIL101 (Fe)@Pt NPs

The MIL101(Fe) NPs and Pt NPs were added into the DMF and made a dispersion with concentration of 2.0×10^{-3} mol/L, 0.6×10^{-3} mol/L, respectively. Then, the Pt NPs dispersion and the MIL101(Fe) NPs dispersion with same volume were mixed together and stirred for 2 h at 45 °C to form homogeneous system. The MIL101 (Fe)@Pt NPs were gained through being centrifuged at 8000 rpm for 10 min. The precipitation was rinsed with DMF solution and ethanol in turn and then centrifuged for three times. The MIL101 (Fe)@Pt NPs were dried under 30 °C for 20 h to discharge excess DMF solvent.

2.6. Preparation of CNTs-PAA/MIL101(Fe)@Pt composite membrane

Firstly, 25 mg of CNTs-PAA was dispersed into 1 L of water. Secondly, different amounts of the CNTs-PAA dispersion (1 mL~20 mL) were put into the filtration setup. A uniform CNTs-PAA composite membrane was got after being vacuum filtrated under 0.1 MPa. Thirdly, 25 mg of MIL101 (Fe)@Pt NPs was dispersed into 1 L of ethanol. Lastly, different volume (5 mL~25 mL) of the MIL101 (Fe)@Pt NPs dispersion were filtrated onto the CNTs-PAA composite membrane under 0.1 MPa.

2.7. Preparation of oil-in-water emulsions and its mixture with water-soluble organic dye

Firstly, 1.0 g of tween 80 was dissolved into 100 mL of distilled water and stirred for 3 h. Secondly, 4 mL of organic solvents (dichloromethane, chloform, hexane, silicon and toluene) were added into above solution and stirred for 8 h, respectively. The as-prepared mixed solution systems were placed undisturbed for 72 h to obtain surfactant stabilized dichloromethane-in-water (D/W) emulsion, chloroform-in-water (C/W) emulsion, hexane-in-water (H/W) emulsion, silicon-in-water (S/W) emulsion and toluene-in-water (T/W) emulsion respectively. MB was taken as a sample for purifying water-soluble organic polluted oily wastewater. 15 mg of MB and 0.15 g of $NaBH_4$ were in turn added into 300 mL of D/W emulsion, T/W emulsion, H/W emulsion, S/W emulsion and then stirred for 5 h to obtain D/M/W mixed emulsion, T/M/W mixed emulsion, H/M/W mixed emulsion and S/M/W mixed emulsion, respectively.

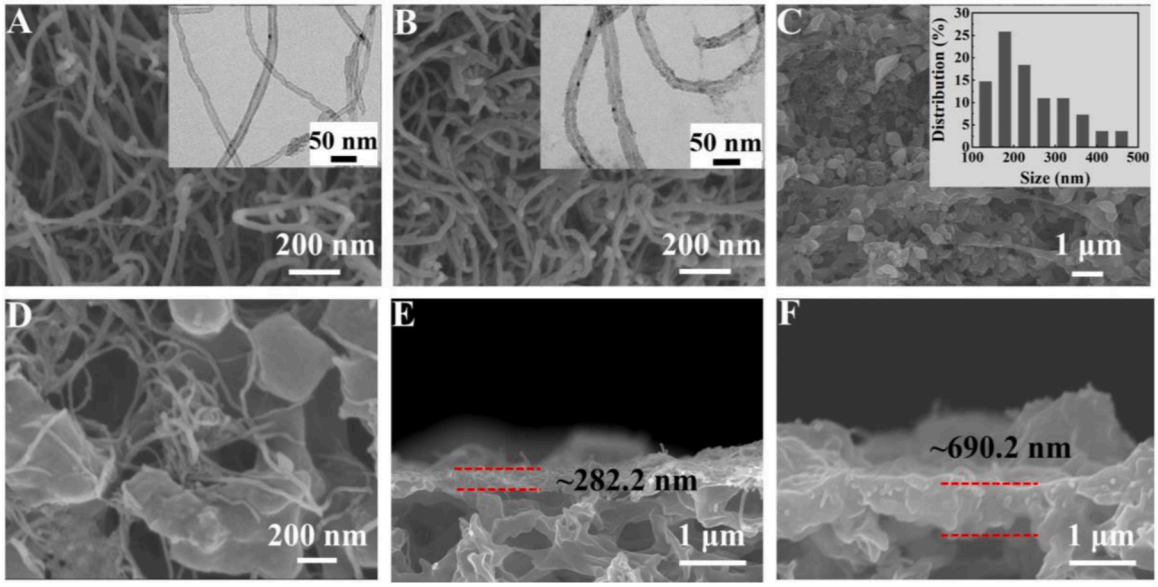

Fig. 2. The SEM images of (A) CNTs membrane and (B) CNT-PAA membrane (Inset: TEM images of CNTs membrane and CNT-PAA membrane, respectively). (C-D) The SEM images of the CNTs-PAA/MIL101(Fe)@Pt composite membrane (Insert: its responding pore diameter distribution). (E-F) The SEM images of the cross-section of the CNTs-PAA membrane and CNTs-PAA/MIL101(Fe)@Pt composite membrane, respectively.

2.8. Separation of surfactant stabilized oil-in-water emulsion

The oil-in-water emulsion separation tests were performed on a vacuum filter apparatus equipped with the CNTs-based composite membrane, where the effective filter area was 11.33 cm^2. In a typical test, 150 mL of oil-in-water emulsions were poured onto the membrane

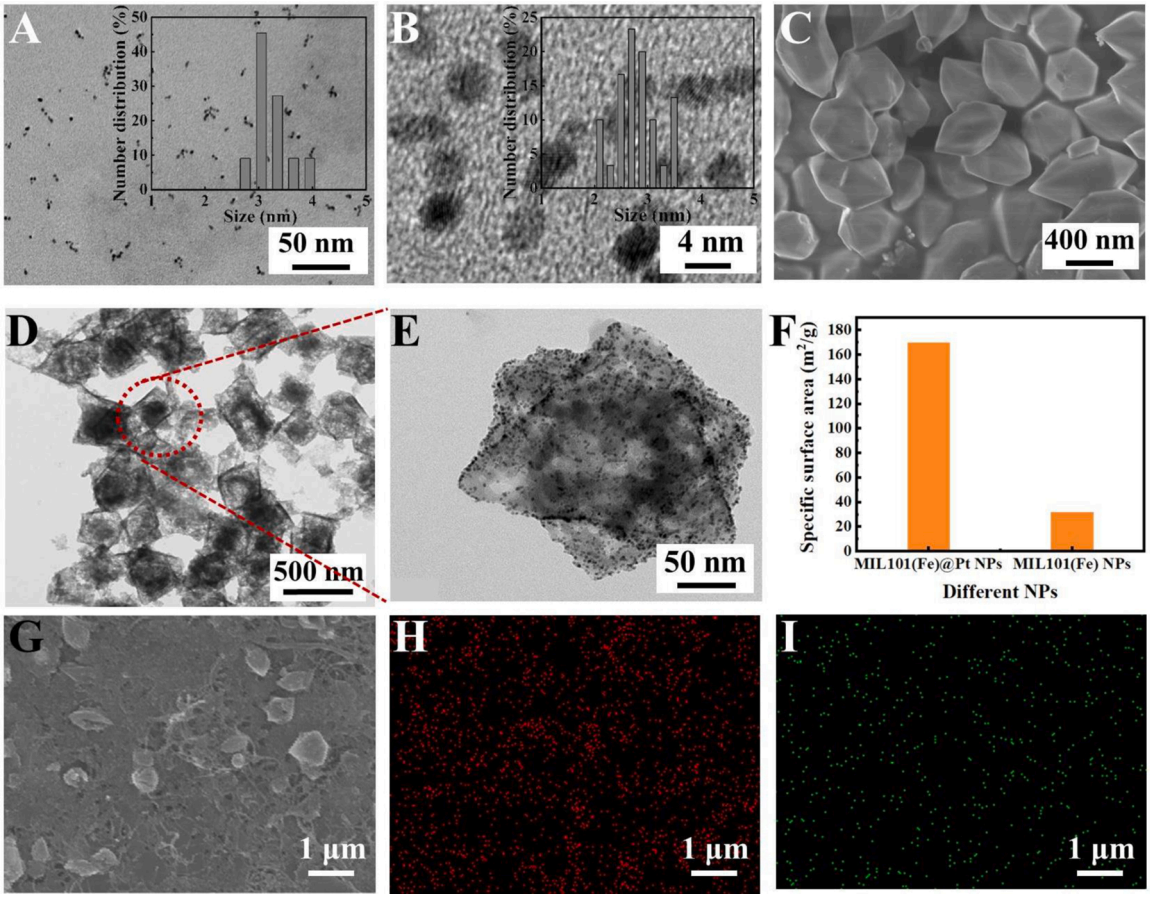

Fig. 3. (A-B) The TEM images of Pt NPs and responding particle size distribution. (C) The SEM image of MIL101(Fe) NPs. (D-E) The TEM image MIL101(Fe)@Pt NPs. (F) The specific surface area of the MIL101(Fe) NPs and MIL101(Fe)@Pt NPs. (G-I) The morphology of the CNTs-PAA/MIL101(Fe)@Pt composite membrane and its responding EDX spectroscopy of Fe (red) and Pt (green).

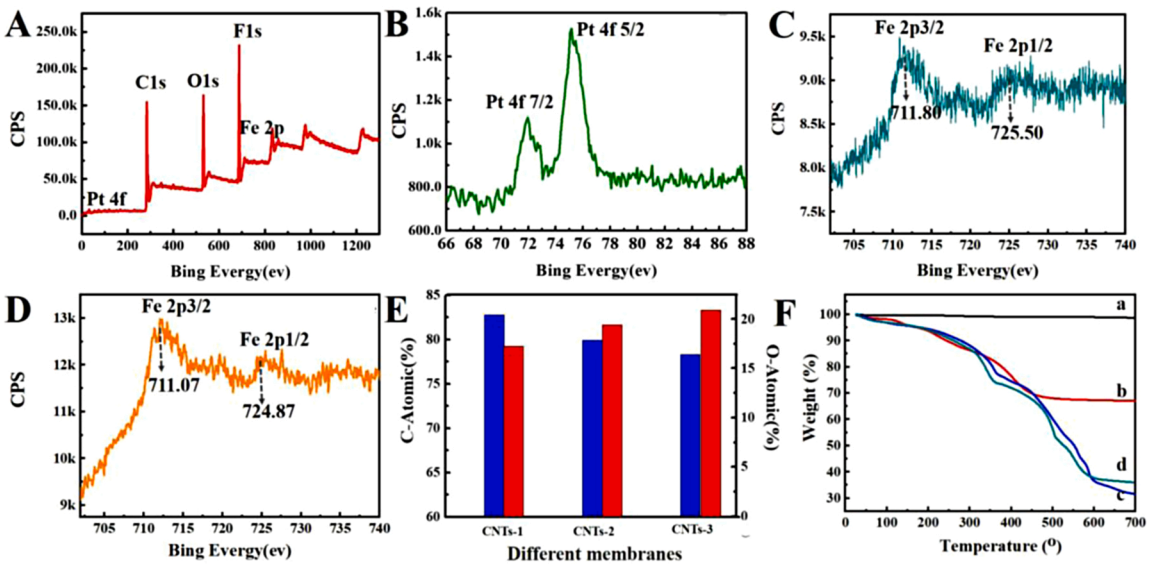

Fig. 4. (A) The XPS spectrum of CNTs-PAA/MIL101(Fe)@Pt composite membrane. (B-C) The Pt 4f and Fe 2p spectrum of the CNTs-PAA/MIL101(Fe)@Pt composite membrane, respectively. (D) The Fe 2p spectrum of the CNTs-PAA/MIL101(Fe) composite membrane. (E) The O 1s and the C 1s mass contents of CNTs-1-CNT-PAA membrane, CNTs-2-CNTs-PAA/MIL101(Fe) composite membrane, CNTs-3-CNTs-PAA/MIL101(Fe)@Pt composite membrane, respectively (blue was C element, red was O element). (E) TGA curves of (a) CNTs, (b) CNTs-PAA, (c) CNTs-PAA/MIL101(Fe) and (d) CNTs-PAA/MIL101(Fe)@Pt.

surface under a pressure of 0.1 MPa.

The separation flux J was calculated according to Eq. (1):

$$J = V/(A \times T) \quad (1)$$

Where V (L) was the filtrate volume, A (m^2) was the effective filtration area, T (h) was the permeate time.

The separation efficiency E was calculated according to Eq. (2):

$$E = (1\text{-}C_b/C_a) \times 100\ \% \quad (2)$$

Where C_a and C_b were the concentration of oil in feed and the filtration, respectively. Concentration was determined by total organic carbon analyzer.

2.9. Catalytic decomposition of water-soluble organic pollutant

MB was set as the representative dye to assess the catalytic decomposition property. A certain amount of MB was filtrated through the CNTs-based composite membrane under a pressure of 0.1 MPa. The feed and filtration were collected for further characterization. The catalytic decomposition efficiency R (%) was calculated according to Eq. (3):

$$R = (1\text{-}C_1/C_o) \times 100\ \% \quad (3)$$

Where C_o and C_1 were the concentration of MB in feed and the filtration, respectively. The concentration was determined by UV/Vis absorption.

2.10. Oil-in-water emulsion separation and catalytic decomposition

A certain amount of oil-in-water emulsion containing water-soluble organic pollutant was filtrated through the CNTs-PAA/MIL101(Fe)@Pt composite membrane under 0.1 MPa. The feed and filtration were collected respectively for further characterization.

2.11. Characterization

Transmission electronic microscopy (TEM) was carried out using a JEOL JEM-2100 F microscope to study the microstructures of the composite membrane. Scanning electronic microscopy (SEM) was performed with a Hitachi S4800 scanning microscope to further characterize its microstructures. Fourier transform infrared (FTIR) spectra were recorded with a Varian Scimitar1000 Fourier transform IR spectrophotometer. Thermogravimetric Analysis (TGA) measurements were performed using a Perkin Elmer STA600 instrument with temperature increase of 10 °C/min under nitrogen atmosphere to evaluate thermal degradation. X-ray photoelectron spectroscopy (XPS) analysis was recorded on a Shimadzu Axis Untraded spectroscope to analyze chemical components. The water contact angles (WCA) and underwater oil contact angles (UOCA) measurements were performed on OCA-20 at room temperature. Dynamic light scattering (DLS) measurements were recorded on a Zetasizer Nano ZS. Optical microscopy images were performed on a CFM-330 microscope by dropping the solution on a wafer. UV/vis absorption spectra were recorded on a TU-1810 UV/vis spectrophotometer. The purification of oil in the feed and filtration were determined by total organic carbon analyzer (TOC).

3. Results and discussions

3.1. Surface morphology and chemical composition

CNTs were functionalized with hydrophilic PAA and formed a dense membrane through vacuum filtration. The surface morphology of the CNTs-PAA before and after MIL101(Fe)@Pt NPs modification were investigated by SEM and TEM. A layer of hydrophilic PAA polymer has attached clearly on the surface of the CNTs and the average diameter of the CNTs increased from ~29 nm to ~55 nm (Fig. 2**A-2B, Fig. S1**). The CNTs-PAA assembled into a uniform porous composite membrane.

To improve the specific surface area of MIL101(Fe)@Pt NPs, a layer of Pt NPs with average diameter of 3 nm (Fig. 3**A-3B, Fig. S2**) were encapsulated densely on the surface of MIL101(Fe). The MIL101(Fe) NPs has presented octahedral structure with the particle size was about 500 nm (Fig. 3C, **Fig. S3**). Furthermore, the MIL101(Fe) NPs retained its initial morphology after Pt NPs modification (Fig. 3**D-3E**). Importantly, the specific surface area of MIL101(Fe) NPs has increased to 170.91 m^2/g (Fig. 3F). The MIL101(Fe)@Pt NPs were decorated into the whole CNT-PAA membrane without remarkable aggregation and partial MIL101(Fe)@Pt NPs were embedded closely inside the membrane network (Fig. 2**C-2D**).The average pore diameter of the CNTs-PAA/MIL101(Fe)@Pt composite membrane was 200~300 nm (Fig. 2D). In addition, the EDX results (Fig. 3**G-3I**) have clearly illustrated the homogeneous distribution of the Fe and Pt elements in the entire composite

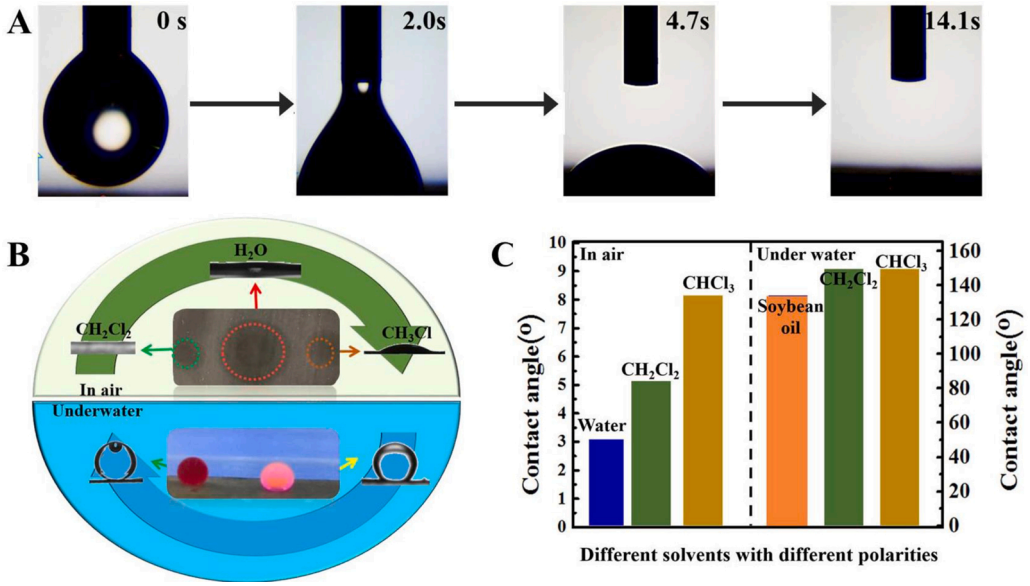

Fig. 5. (A) Dynamic WCA of the composite membranes when a water droplets spreads on the interface of the CNTs-PAA/MIL101(Fe)@Pt composite membrane. (B-C) The CA of different solvents on the CNTs-PAA/MIL101(Fe)@Pt composite membranes in air and underwater.

membrane, which have further proved that the MIL101(Fe)@Pt NPs were uniformly coated on the CNT-PAA composite membrane. The SEM image of the cross-section of the CNTs-PAA/MIL101(Fe)@Pt composite membrane has indicated that it has interlaced into a compacted network membrane with an average thickness of about 690 nm (Fig. 2F), which was higher than that of the CNTs-PAA membrane (Fig. 2E**, Fig. S4**).

The attachment of MIL101(Fe)@Pt NPs were further confirmed by XPS. As shown in **Fig. S5A-S5C,** there was a strong Fe 2p peak at ~711 eV in the XPS spectrum of the CNTs-PAA/MIL101(Fe) composite membrane, and whereas there was no Fe 2p peak in the CNTs-PAA membrane. The XPS results of CNTs-PAA/MIL101(Fe)@Pt composite membrane revealed the Pt 4f peak at ~74 eV and Fe 2p peak at ~711 eV (Fig. 4**A-4C**), which proved the modification of MIL101(Fe)@Pt NPs on the surface of CNTs-PAA membrane. Moreover, the peaks at 711.07 eV and 724.87 eV were the characteristic peaks of Fe 2p3/2 and Fe 2p1/2, which can prove the existence of Fe-O bonds in CNTs-PAA/MIL101(Fe)@Pt (Li et al., 2016c). However, due to a partial transfer of electrons from the Pt NPs to MIL101(Fe) NPs (Garca et al., 2019) and resulting in the reduction of electron density, the absorption peak Fe 2p of CNTs-PAA/MIL101(Fe) has shifted toward short wavenumber (Fig. 4D). In addition, The C 1s mass content of CNTs-PAA membrane (**Fig. S5D**) was higher than that of the CNTs-PAA/MIL101(Fe)@Pt composite membrane (**Fig. S5F**). On the contrary, the O 1s mass contents has presented opposite trend (**Fig. S5G**, **S5I**). The C/O mass ratio has declined from 4.797 to 3.738 (Fig. 4E**).** These results provided the successful attachment of MIL101(Fe)@Pt NPs on the CNTs-PAA membrane. The functionalization of PAA and the attachment of MIL101(Fe)@Pt NPs on the surface of CNTs were also confirmed by TGA (Fig. 4F). The weight loss of the pristine purified CNTs at 700 °C under nitrogen was only 2.2 wt%. With respect to CNTs-PAA membrane, two main weight-loss regions were found. The first weight-loss region may be assigned to the decomposition of carboxyl groups of PAA on the surface of CNTs and the significant weight reduction in the second region was due to the decomposition of the polymer backbone and hydroxyethyl groups (Zhang et al., 2016a). In addition, the weight loss of the CNTs-PAA/MIL101(Fe) composite was higher than that of the CNTs-PAA/MIL101(Fe)@Pt composite, indicating the relatively low content of Pt NPs.

3.2. Surface wettability

WCA measurements were taken to investigate the surface wettability of CNTs membrane before and after nanoparticles attachment. According to Wenzel model and Cassie-Baxter model (Liu et al., 2019), the surface morphology and chemical composition determine the surface energy and further endow the surface with special wettability. In the liquid/air/solid three-phase system, the WCA of CNTs membrane reduced from ~67° to ~18° after the modification of PAA due to the large number of carboxyl groups on the surface of CNTs-PAA membrane (**Fig. S6**). The influence of the relative amount of the MIL101(Fe)@Pt NPs on the wettability of the CNTs-PAA/MIL101(Fe)@Pt composite membrane was further investigated. As shown in Fig. S7, this composite membrane has shown superoleophobicity underwater when the dosage of the MIL101(Fe)@Pt NPs was appropriate, which can be explained by the Wenzel's model that surface roughness can promote surface wettability (Li et al., 2018b). Based on this, we studied the wettability of CNTs-PAA/MIL101(Fe)@Pt composite membrane in air and under water. As shown in Fig. 5A, the water droplets spread rapidly on the surface of composition membrane with WCA about 3° (Fig. 5**A and B**). In addition, the CNTs-PAA/MIL101(Fe)@Pt composite membrane has presented similar oleophilic wettability with the OCA less than 9° (Fig. 5B). These results indicated the superamphiphilic property of this composite membrane. Inversely, the CNTs-PAA/MIL101(Fe)@Pt composite membrane has displayed underwater superoleophobic property with the UOCA more than 150° for all investigated oil droplets (Fig. 5**B and C**). The special surface wettability endowed this composite membrane a promising alternative for the separation of oil-in-water emulsion.

3.3. Oil-in-water emulsion separation performance

The unique wettability allowed the obtained composite membrane a good candidate for selectively separating oil from water. Firstly, we investigated the effect of the amount of the MIL101(Fe)@Pt NPs on the separation performance for D/W emulsion. As shown in **Fig. S8**, the separation flux has gradually decreased along with the increasing amount of MIL101(Fe)@Pt NPs dispersion. This was due to the volume of dispersion was positively correlated with the membrane thickness in the process of filtration (Zhang et al., 2020). Secondly, the influence of the volume usage of the CNTs-PAA solution on the separation

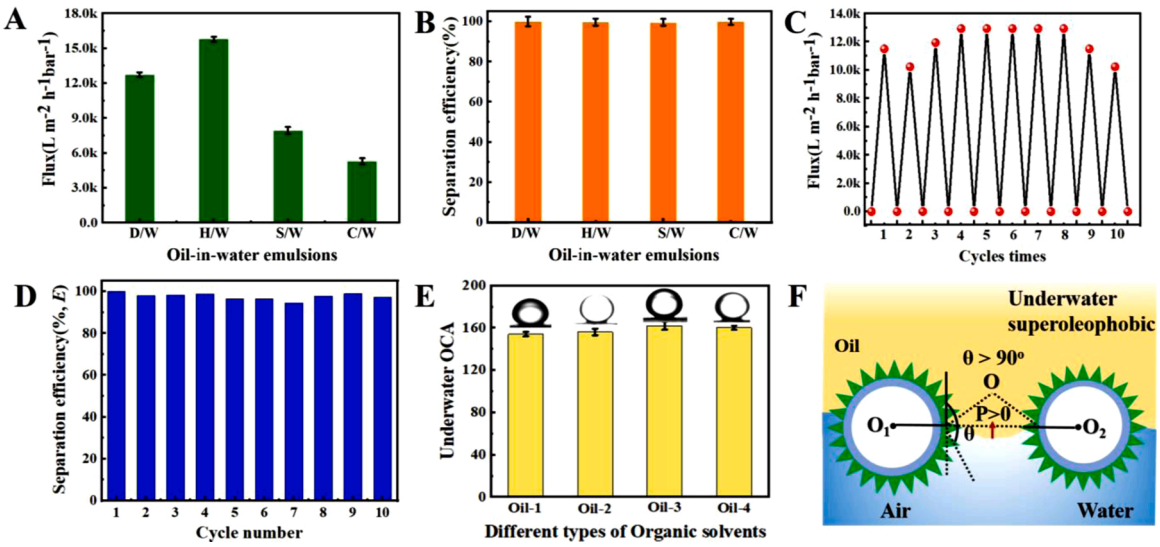

Fig. 6. (A-B) The separation flux and efficiency of the CNTs-PAA/MIL101(Fe)@Pt composite membrane for various oil-in-water emulsions. (C-D) The cyclic separation flux and efficiency for D/W emulsion. (E) The UOCA of the CNTs-PAA/MIL101(Fe)@Pt composite membrane according to different types of organic solvents (from left to right: chloroform, dichloromethane, 1, 2-dichloroethane, tetrachloromethane). (F) Schematic illustration of the separation of oil-in-water emulsion of the CNTs-PAA/MIL101(Fe)@Pt composite membrane.

performance of this composite membrane was further studied. As shown in **Fig. S9**, the separation flux was negatively related to the amount of CNTs-PAA solution. The lower volume of the CNTs-PAA solution has brought weak separation stability of this composite membrane, which resulted in the several breaks after only one cycle emulsion separation. Whereas, the longer and tortuous separation paths were not is not conducive to enhance the separation flux. In order to balance the trade-off the separation flux and the efficiency of this composite membrane, the most suitable dosage of the CNTs-PAA solution was 10 mL. Under this case, a series of oil-in-water emulsions (D/W emulsion, H/W emulsion, S/W emulsion, C/W emulsion) were taken as examples evaluate the separation ability of the CNTs-PAA/MIL101(Fe)@Pt composite membrane. The de-emulsification occurred once the oil-in-water emulsion touching the upper surface of the CNTs-PAA/MIL101(Fe)@Pt composite membrane, and the water droplets immediately passed through whereas the oil phase was retained above the membrane. Optical microscopy and DLS were employed to characterize the oil droplets in the feed and filtration to assess the separation efficacy. As shown in **Fig. S10-S11**, a huge amount of densely packed oil droplets with micro-size in the feed solution disappeared and only oil droplets with sizes below 30 nm were observed in the filtrate in the entire view, showing the excellent emulsion separation ability of the CNTs-PAA/MIL101(Fe)@Pt composite membrane. The purity of the oil in the feed and filtration were also quantitatively tested by TOC. The purities were above 99.79 % for all the investigated oil-in-water emulsions, indicating the extremely good separation effectiveness of the CNTs-PAA/MIL101(Fe)

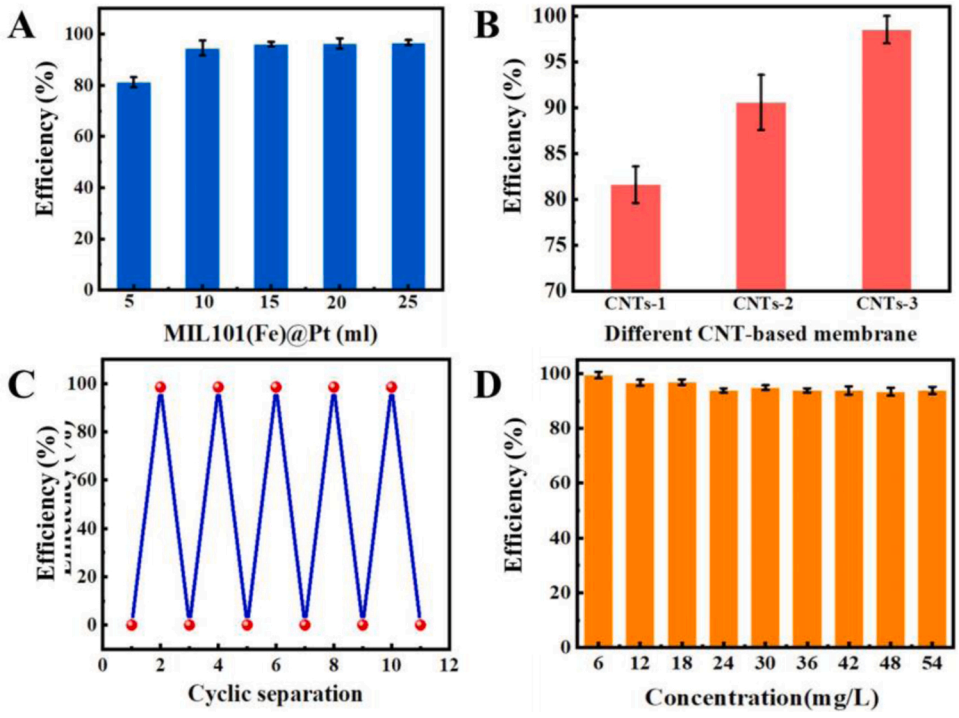

Fig. 7. (A) The influence of the dosages of MIL101(Fe)@Pt NPs on the adsorption and degradation efficiency for MB. (B) The adsorption and degradation efficiency of different CNT-based membranes (CNT-1-CNT-PAA membrane, CNTs-2-CNTs-PAA/MIL101(Fe) membrane, CNTs-3-CNTs-PAA/MIL101(Fe)@Pt membrane). (C) The cyclic adsorption and degradation efficiency of the MB solution using the CNTs-PAA/MIL101(Fe)@Pt composite membrane. (D) The adsorption and degradation efficiency of the CNTs-PAA/MIL101(Fe)@Pt composite membrane for MB with different initial concentrations.

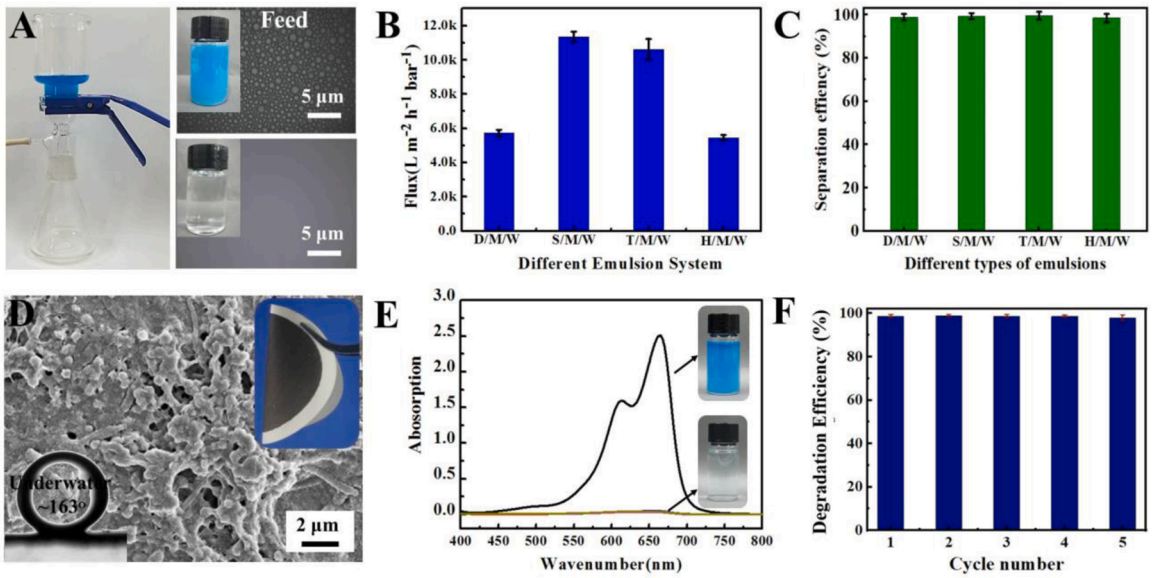

Fig. 8. (A) A photograph of the filtration setup for oil-in-water emulsions separation meanwhile catalytic degradation of MB permeating through the CNTs-PAA/MIL101(Fe)@Pt composite membrane (Inserting: the optical microscopy of emulsions before and after separation). The separation flux (B) and efficacy (C) for different types of oil-in-water emulsions containing MB of the CNTs-PAA/MIL101(Fe)@Pt composite membrane. (D)The wettability and microstructure of the CNT-PAA/MIL101(Fe)@Pt composite membrane after five cycles of purification. (E) The UV/vis absorption and the photographs of the feed emulsion and filtrate before and after separation. (F) The cyclic catalytic decomposition ability of oil-in-water emulsion containing MB.

@Pt composite membrane. The membrane permeating flux of various oil-in-water emulsions were comprehensively investigated. As shown in the Fig. 6A, all the D/W, H/W S/W and C/W have shown high separation flux with 12,744 ± 204, 15,784 ± 364, 7939 ± 220, and 5293 ± 286 L m^{-2} h^{-1} bar^{-1}, respectively. Moreover, this composite membrane has presented excellent separation efficiency for various emulsions (Fig. 6B). In addition, the reliability of this composite membrane was evaluated by carrying out cyclic separation of D/W emulsion. As shown in Fig. 6**C-6D**, the separation flux and efficiency did not show remarkable changes during ten cycles of separation. Furthermore, the CNTs-PAA/MIL101 (Fe)@Pt composite membrane kept its wettability even after ten cycles of separation (Fig. 6E). These results have proved the potential application performance of the CNTs-PAA/MIL101(Fe)@Pt composite membrane. On the basis of the experimental results of oil-in-water separation, the mechanism was proposed and illustrated in Fig. 6**F**. A hydrophilic lay will formed once the oil-in-water emulsion touching the membrane surface due to the superhydrophilic and underwater superoleophobic of the CNTs-PAA/MIL101(Fe)@Pt composite membrane. When the applied pressure across the membrane was larger than the force between surfactants and water molecules (P > 0) (An et al., 2018; Li et al., 2016a), the de-emulsification occurred and the continuous water phase could easily permeate through the membranes whereas the dispersed oil phase was repulsed.

3.4. Dye catalytic decomposition ability

Catalytic degradation is an advisable way to remove water-soluble organic contaminants (Zhang et al., 2016a). In this work, MB was chose as a representative mode to evaluate the catalytic performance of CNTs-PAA/MIL101(Fe)@Pt composite membrane. Firstly, we studied the adsorption capacity of the CNT-PAA/MIL101(Fe)@Pt composite membrane for MB. As shown in **Fig. S12**, its adsorption capacity has increased gradually until reached the maximum (~66.5 %). Secondly, the influence of different dosages of MIL101(Fe)@Pt NPs on the adsorption and degradation efficiency for MB were explored. As shown in Fig. 7A, with the increasing volume of MIL101(Fe)@Pt NPs dispersion, its adsorption and degradation ability has increased until it attained to 98.5 %. Furthermore, the adsorption and degradation efficiency of different membranes was further investigated. As shown in Fig. 7B, the CNT-PAA membrane has shown a good adsorption and degradation efficiency by coupling with MIL101(Fe) NPs. It was noting that the addition of Pt NPs can achieve significantly photocatalytic activity of CNTs-PAA/MIL101(Fe) composite membrane. The MIL101(Fe) @Pt NPs can act as a co-catalyst to prolong the lifetime of energetic charge carriers by boosting the separation of electron-hole on the co-catalyst interface (Mateo et al., 2019). Moreover, the adsorption and degradation efficiency of the CNT-PAA/MIL101(Fe)@Pt composite membrane has changed within 1–3 % (Fig. 7C) after five cycles and it has been hardly affected regardless of the initial concentration of MB (Fig. 7D), which indicated the excellent reusability of the CNTs-PAA/MIL101(Fe)@Pt composite membrane and the stable modification of MIL101(Fe)@Pt NPs. Two key factors have significant influenced on the adsorption and degradation performance of the CNTs-PAA/MIL101(Fe)@Pt composite membrane. One was that the special wettability of this composite membrane has facilitated the effective contact between MB and membrane interface. The other was that MIL101(Fe)@Pt NPs were excited and reactive electron-hole pairs with strong redox activity were generated (Zhang et al., 2016b). These processes generated highly reactive radicals' species, which degraded the organic contaminants in water.

3.5. Synchronization of catalytic decomposition and emulsion separation

The CNTs-PAA/MIL101(Fe)@Pt composite membrane associating the catalytic degradation of dyes and the separation of oil-in-water emulsion is regard as a promising candidate to achieve flow-through purification oily wastewater. To prove the practicability of the CNTs-PAA/MIL101(Fe)@Pt composite membrane, different types of oil-in-water emulsions containing MB in water (D/M/W emulsion, S/M/W emulsion, T/M/W emulsion, H/M/W emulsion) were used to simulate organic dye molecules polluting oily wastewater. In this work, the separation of mixed blue emulsion was setup under 0.1 MPa (Fig. 8A). The feed emulsion kept blue until it passed through the CNTs-PAA/MIL101 (Fe)@Pt composite membrane. Optical microscopy and DLS results manifested that numerous droplets with size at a micron- scale in the feed solution disappeared and only nano-sized droplets were observed in

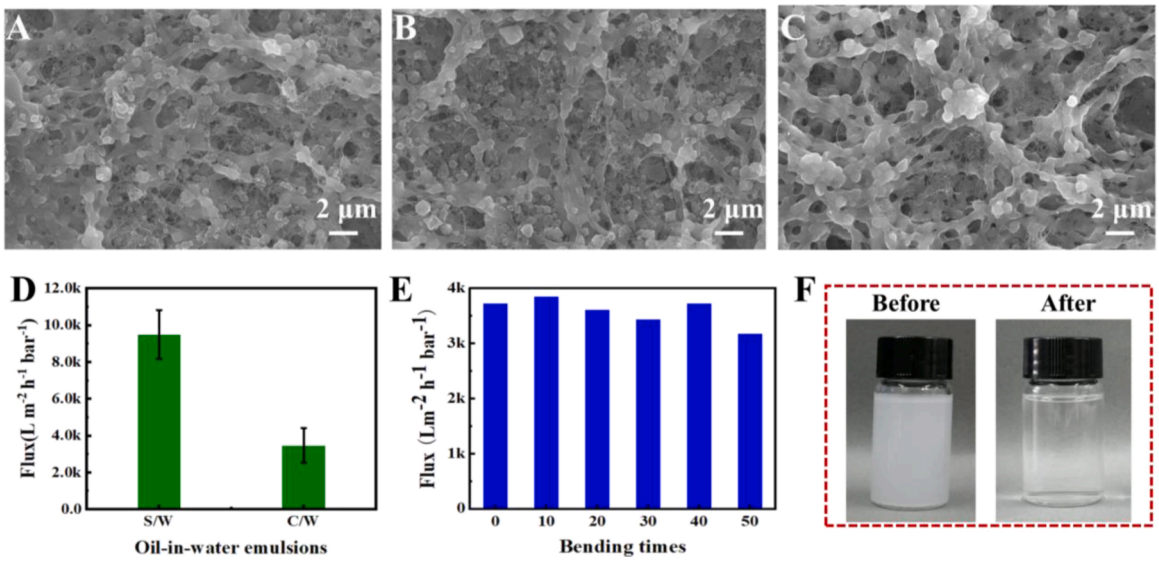

Fig. 9. The SEM images of the CNTs-PAA/MIL101(Fe)@Pt composite membrane after being immerged in the (A) HCl solution, (B) NaOH solution and (C) NaCl solution for 24 h. (D) The separation flux of the various oil-in-water emulsions after being immerged in the NaCl solution for 7 days. (E) The separation flux of T/W emulsion after several times bending. (F) The photographs of the T/W emulsion before and after being separated with the bent CNTs-PAA/MIL101(Fe)@Pt composite membrane for 50 times.

the filtrate (Fig. 8**A** and **Fig. S13**). Meanwhile, the separation flux of various emulsions permeating through the cross membrane were calculated through measuring the flow volume at fixed time and valid area. As shown in Fig. 8B, the maximum flux of the CNTs-PAA/MIL101 (Fe)@Pt composite membrane can reach up to about 11,000 L m^{-2} h^{-1} bar^{-1}, which has exceeded the majority of the previously reported multi-functional membranes (**Table S1**). The separation efficiency for all the tested mixed emulsions was above 98.8 %, indicating its high separation efficiency (Fig. 8**C**). The CNTs-PAA/MIL101(Fe)@Pt composite membrane kept its wettability and there was no obvious in microstructure after five cycles of the mixed emulsions separation (Fig. 8**D**). Furthermore, it was worth noting that the absorption of MB at 660 nm was only reduced 2.4 % of the initial absorption after catalytic decomposition (Fig. 8**E**) and the separation efficacy maintained above 98.5 % after five cycles of separation (Fig. 8**F**), demonstrating the unique flow-through catalysis performance of the CNTs-PAA/MIL101(Fe)@Pt composite membrane. The good recyclability and durability as well as the outstanding catalytic decomposition performance made this membrane a promising candidate for purifying oily wastewater.

3.6. Physical and chemical stability

The stability of a filtration membrane is important for further practical application. The durability of the CNTs-PAA/MIL101(Fe)@Pt composite membrane was tested by monitoring the microstructure before and after being immerged in the hydrochloric acid (HCl, pH = 1) solution, sodium hydroxide (NaOH, pH = 13) solution and sodium chloride (NaCl, 0.1 mol/L) solution for 24 h. As shown in Fig. 9**A-9C**, this composite membrane maintained its original micro/nanostructure. Moreover, the composite membrane has presented emulsion separation performance towards various O/W emulsions (Fig. 9D). In addition, the CNTs-PAA/MIL101(Fe)@Pt composite membrane has shown stable structure, separation flux and the filtration was transparent even it was bent for 50 times (Fig. 9**E-9F, Fig. S14**). These results have proved the CNTs-PAA/MIL101(Fe)@Pt composite membrane has excellent physical and chemical stability.

4. Conclusions

In summary, a facile method to construct multifunctional CNTs-PAA/MIL101(Fe)@Pt composite membranes through hydrophilic PAA functionalization and afterwards octahedral MIL101(Fe)@Pt modification has been presented. The achieved CNTs-PAA/MIL101(Fe)@Pt composite membrane was possessed with superhydrophilicity and underwater superoleophobicity under the synergistic effect of CNT-PAA composite membrane and MIL101(Fe)@Pt NPs. The obtained composite membrane can synchronously realize the catalytic degradation of above 98.5 % dye molecule in oily water and oil-in-water emulsion separation with separation efficiency approach to 98.8 %. Furthermore, the multifunctional composite membrane has presented a separation flux as high as 11,000 L m^{-2} h^{-1} bar^{-1}, which has surpassed the most of the previously reported multi-functional separation membrane. Importantly, it has shown outstanding durability and catalytic recyclability. Therefore, we hope this work can provide a new platform to design multifunctional carbon-based membranes for practical wastewater purification.

Declaration of Competing Interest

The authors report no declarations of interest.

Acknowledgements

We gratefully acknowledge the support from Open Research Fund of Key Laboratory of Marine Materials and Related Technologies (2017K03), the Bureau of Frontier Science and Education of Chinese Academy of Sciences (QYZDB-SSW-SLH036), Ningbo Science and Technology Bureau (2018A610097), Special Fund for Basic Scientific Research of Central Colleges, Chang' an University (300102318403, 300102319306).

Declaration of competing Interest

The authors declare that they have no known competing financial interests or personal relationships that could have appeared to influence the work reported in this paper.

Appendix A. Supplementary data

Supplementary material related to this article can be found, in the online version, at doi:https://doi.org/10.1016/j.jhazmat.2020.123547.

References

An, Y.P., Yang, J., Yang, H.C., Wu, M.B., Xu, Z.K., 2018. Green synthesis of fluorescent carbon dots from gynostemma for bioimaging and antioxidant in zebrafish. ACS Appl. Mater. Interfaces 11, 9832–9840. https://doi.org/10.1021/acsami.9b00074.

Cao, G.L., Wang, Y.G., Wang, C.Y., Ho, S.H., 2019. Dually prewetted membrane for continuous filtration of water-in-light oil, oil-in-water, and water-in-heavy oil multiphase emulsion mixtures. J. Mater. Chem. A 7, 11305–11313. https://doi.org/10.1039/C9TA01889A.

Chen, F., Lu, Y., Liu, X., Song, J.L., He, G.J., Tiwari, M.K., Carmalt, C.J., Parkin, I.P., 2017. Oil/water separation: table salt as a template to prepare reusable porous PVDF-MCNT foam for separation of immiscible oils/organic solvents and corrosive aqueous solutions. Adv. Funct. Mater. 41 https://doi.org/10.1002/adfm.201702926, 2017 02926.

Duan, C.T., Zhu, T., Guo, J., Wang, Z., Liu, X.F., Wang, H., Xu, X., Jin, Y., Zhao, N., Xu, J., 2015. Smart enrichment and facile separation of oil from emulsions and mixtures by superhydrophobic/superoleophilic particles. ACS Appl. Mater. Interfaces 7, 10475–10481. https://doi.org/10.1021/acsami.5b01901.

Dutta, K., De, S., 2017. Smart responsive materials for water purification: an overview. J. Mater. Chem. A 5, 22095–22112. https://doi.org/10.1039/C7TA07054C.

Fang, Y., Powell, J.A., Li, E., Wang, Q., Perry, Z., Kirchon, A., Yang, X., Xiao, Z., Zhu, C., Zhang, L., Huang, F., Zhou, H.C., 2019. Catalytic reactions within the cavity of coordination cages. Chem. Soc. Rev. 48, 4707–4730. https://doi.org/10.1039/C9CS00091G.

Feng, L., Zhang, Z., Mai, Z., Ma, Y., Liu, B., Jiang, L., Zhu, D., 2004. A super-hydrophobic and super-oleophilic coating mesh film for the separation of oil and water. Angew. Chem. Int. Ed. 43, 2012–2014. https://doi.org/10.1002/ange.200353381.

Fu, Y.C., Jin, B.Y., Zhang, Q.H., Zhan, X.L., Chen, F.Q., 2017. pH-Induced switchable superwettability of efficient antibacterial fabrics for durable selective oil/water separation. ACS Appl. Mater. Interfaces 9, 30161–30170. https://doi.org/10.1021/acsami.7b09159.

Gao, S.J., Zhu, Y.Z., Zhang, F., Jin, J., 2015. Superwetting polymer-decorated SWCNT composite ultrathin films for ultrafast separation of oil-in-water nanoemulsions. J. Mater. Chem. A 3, 2895–2902. https://doi.org/10.1039/C4TA05624H.

Ge, J., Zhao, H.Y., Zhu, H.W., Huang, J., Shi, L.A., Yu, S.H., 2016. Advanced sorbents for oil-spill cleanup: recent advances and future perspectives. Adv. Mater. 28, 10459–10490. https://doi.org/10.1002/adma.201601812.

Gong, Y., Yang, B., Zhang, H., Zhao, X., 2018. A g-C_3N_4/MIL101(Fe) heterostructure composite for highly efficient BPA degradation with persulfate under visible light irradiation. J. Mater. Chem. A 6, 23703–23711. https://doi.org/10.1039/C8TA07915C.

Gu, J.C., Xiao, P., Chen, J., Liu, F., Huang, Y.J., Li, G.Y., Zhang, J.W., 2014a. Robust preparation of superhydrophobic polymer/ carbon nanotube hybrid membranes for highly effective removal of oils and separation of water-in-oil emulsions. J. Mater. Chem. A 2, 15268–15272. https://doi.org/10.1039/C4TA01603C.

Gu, J.C., Xiao, P., Chen, J., Zhang, J.W., Huang, Y.J., Chen, T., 2014b. Janus polymer/carbon nanotube hybrid membranes for oil/water separation. ACS Appl. Mater. Interfaces 6, 16204–16209. https://doi.org/10.1021/am504326m.

Gu, J.C., Xiao, P., Huang, Y.J., Zhang, J.W., Chen, T., 2015. Controlled functionalization of carbon nanotubes as superhydrophobic material for adjustable oil/water separation. J. Mater. Chem. A 3, 4124–4128. https://doi.org/10.1039/C4TA07173E.

Gupta, P., Kandasubramanian, B., 2017. Directional fluid gating by Janus membranes with heterogeneous wetting properties for selective oil-water separation. ACS Appl. Mater. Interfaces 9, 19102–19113. https://doi.org/10.1021/acsami.7b03313.

Hu, L., Gao, S.J., Zhu, Y.Z., Zhang, F., Jiang, L., Jin, J., 2015. An ultrathin bilayer membrane with asymmetric wettability for pressure responsive oil/water emulsion separation. J. Mater. Chem. A 3, 23477–23482. https://doi.org/10.1039/C5TA03975D.

Li, J., Kang, R.M., Tang, X.H., She, H.D., Yang, Y.X., Zha, F., 2016a. Superhydrophobic meshes that can repel hot water and strong corrosive liquids used for efficient gravity-driven oil/water separation. Nanoscale 8, 7638–7645. https://doi.org/10.1039/C6NR01298A.

Li, Y.F., Jin, R.X., Xing, Y., Li, J.Q., Song, S.Y., Liu, X.C., Li, M., Jin, R.C., 2016b. Macroscopic foam-like holey ultrathin g-C_3N_4 nanosheets for drastic improvement of visible-light photocatalytic activity. Adv. Energy Mater. 6, 1601273 https://doi.org/10.1002/aenm.201601273.

Li, J., Li, D.M., Yang, Y.X., Li, J.P., Zha, F., Lei, Z.Q., 2016. A prewetting induced underwater superoleophobic or underoil (super) hydrophobic waste potato residue-coated mesh for selective efficient oil/water separation. Green Chem. 18, 541–549. https://doi.org/10.1039/C5GC01818H.

Li, F.R., Wang, Z.R., Huang, S.C., Pan, Y.L., Zhao, X.Z., 2018a. Flexible, durable, and unconditioned superoleophobic/superhydrophilic surfaces for controllable transport and oil-water separation. Adv. Funct. Mater. 28, 1706867 https://doi.org/10.1002/adfm.201706867.

Li, J.J., Zhou, Y.N., Luo, Z.H., 2018b. Polymeric materials with switchable superwettability for controllable Oil/water separation: a comprehensive review. Prog. Polym. Sci. 87, 1–33. https://doi.org/10.1016/j.progpolymsci.2018.06.009.

Liu, N., Zhang, M., Zhang, W.F., Cao, Y.Z., Chen, Y.N., Lin, X., Xu, L.X., Li, C., Feng, L., Wei, Y., 2015. Ultralight free-standing reduced graphene oxide membranes for oil-in-water emulsion separation. J. Mater. Chem. A 3, 20113–20117. https://doi.org/10.1039/C5TA06314K.

Liu, J.C., Wang, N., Yu, L.J., Karton, A., Li, W., Zhang, W.X., Guo, F.Y., Li, L., Cheng, Q.F., Jiang, L., Weitz, D.A., Zhao, Y., 2017. Bioinspired graphene membrane with temperature tunable channels for water gating and molecular separation. Nat. Commun. 8, 17021985 https://doi.org/10.1038/s41467-017-02198-5.

Liu, Y.N., Su, Y.L., Cao, J.L., Guan, J.Y., Xu, L.Y., Zhang, R.N., He, M.R., Zhang, Q., Fan, L., Jiang, Z.Y., 2018. Asymmetric aerogel membranes with ultrafast water permeation for the separation of oil-in-water emulsion. ACS Appl. Mater. Interfaces 10, 26546–26554. https://doi.org/10.1021/acsami.8b09362.

Mateo, D., Portillo, A.S., Albero, J., Navalln, S., Alvaro, M., Garca, H., 2019. Long-term photostability in terephthalate metal-organic frameworks. Angew. Chem. Int. Ed. 58, 17843–17848. https://doi.org/10.1002/ange.201911600.

Meng, F.N., Zhang, M.Q., Ding, K., Zhang, T., Gong, Y.K., 2018. Cell membrane mimetic PVDF microfiltration membrane with enhanced antifouling and separation performance for oil/water mixtures. J. Mater. Chem. A 6, 3231–3241. https://doi.org/10.1039/C7TA10135J.

Mi, H.Y., Jing, X., Huang, H.X., Turng, L.S., 2017. Controlling superwettability by microstructure and surface energy manipulation on three-dimensional substrates for versatile gravity-driven oil/water separation. ACS Appl. Mater. Interfaces 9, 37529–37535. https://doi.org/10.1021/acsami.7b10901.

Shi, Z., Zhang, W.B., Zhang, F., Liu, X., Wang, D., Jin, J., Jiang, L., 2013. Ultrafast separation of emulsified oil/water mixtures by ultrathin free-standing SWCNT network films. Adv. Mater. 25, 2422–2427. https://doi.org/10.1002/adma.201204873.

Song, Y.Y., Zhou, J.J., Fan, J.B., Zhai, W.Z., Meng, J.X., Wang, S.T., 2018. Hydrophilic/oleophilic magnetic Janus particles for the rapid and efficient oil-water separation. Adv. Funct. Mater. 28, 1802493 https://doi.org/10.1002/adfm.201802493.

Wang, B., Liang, W.X., Guo, Z.G., Liu, W.M., 2015. Biomimetic super-lyophobic and super-lyophilic materials applied for oil/water separation: a new strategy beyond nature. Chem. Soc. Rev. 44, 336–361. https://doi.org/10.1039/C4CS00220B.

Wang, Z.X., Lau, C.H., Zhang, N.Q., Bai, Y.P., Shao, L., 2015. Mussel-inspired tailoring of membrane wettability for harsh water treatment. J. Mater. Chem. A 3, 2650–2657. https://doi.org/10.1039/C4TA05970K.

Wang, B., Liu, Y., Zhang, Y.B., Guo, Z.G., Zhang, H., Xin, J.H., Zhang, L., 2015c. Bioinspired superhydrophobic Fe_3O_4@polydopamine@Ag hybrid nanoparticles for liquid marble and oil spill. Adv. Mater. Interfaces 2. https://doi.org/10.1002/admi.201500234, 201500234.

Wang, Y.S., Wang, Y., Xia, H., Wang, G., Zhang, Z.Y., Han, D.D., Lv, C., Feng, J., Sun, H. B., 2016. Preparation of a Fe_3O_4-Au-GO nanocomposite for simultaneous treatment of oil/water separation and dye decomposition. Nanoscale 8, 17451–17457. https://doi.org/10.1039/C6NR05633D.

Wang, X.L., Pan, Y.M., Shen, C.Y., Liu, C.T., Liu, X.H., 2018. Facile thermally impacted water-induced phase separation approach for the fabrication of skin-free thermoplastic polyurethane foam and its recyclable counterpart for oil-water separation. Macromol. Rapid Commun. 39, 1800635 https://doi.org/10.1002/marc.201800635.

Wang, K.D., Wu, C., Wang, F., Liu, C.M., Yu, C.J., Jiang, G.Q., 2018. In-situ insertion of carbon nanotubes into metal-organic frameworks-derived a-Fe_2O_3 polyhedrons for highly sensitive electrochemical detection of nitrite. Electrochim. Acta 285, 128–138. https://doi.org/10.1016/j.electacta.2018.07.228.

Wang, X.L., Pan, Y.M., Liu, X.H., Liu, H., Li, N., Liu, C.T., Schubert, D.W., Shen, C.Y., 2019. Facile fabrication of superhydrophobic and eco-friendly poly(lactic acid) foam for oil-water separation via skin peeling. ACS Appl. Mater. Interfaces 11, 14362–14367. https://doi.org/10.1021/acsami.9b02285.

Wang, F., Luo, S.H., Xiao, S.B., Zhang, W.J., Zhuo, Y.Z., He, J.Y., 2020a. Enabling phase transition of infused lubricant in porous structure for exceptional oil/water separation. J. Hazard. Mater. 390, 122176 https://doi.org/10.1016/j.jhazmat.2020.122176.

Wang, X.L., Pan, Y.M., Yuan, H., Su, M., Shao, C.G., Liu, C.T., Guo, Z.H., Shen, C.Y., Liu, X.H., 2020. Simple fabrication of superhydrophobic PLA with honeycomb-like structures for high-efficiency oil-water separation. Chin. Chem. Lett. 31, 365. https://doi.org/10.1016/j.cclet.2019.07.044.

Wei, C.J., Dai, F.Y., Lin, L.G., An, Z.H., He, Y., Chen, X., Chen, L., Zhao, Y.P., 2018. Simplified and robust adhesive-free superhydrophobic SiO_2-decorated PVDF membranes for efficient oil/water separation. J. Mater. Sci. 555, 220–228. https://doi.org/10.1016/j.memsci.2018.03.058.

Xie, A.T., Cui, J.Y., Yang, J., Chen, Y.Y., Dai, J.D., Lang, J.H., Li, C.X., Yan, Y.S., 2019. Photo-fenton self-cleaning membranes with robust flux recovery for an efficient oil/water emulsion separation. J. Mater. Chem. A 7, 8491–8502. https://doi.org/10.1039/C9TA00521H.

Yan, L.K., Zhang, G., Zhang, L., Zhang, Gu, Huang, J.C., Zhang, Y.J., Chen, J.W., 2019. Robust construction of underwater superoleophobic CNTs/nanoparticles multifunctional hybrid membranes via interception effect for oily wastewater purification. J. Membrane Sci. 569, 32–40. https://doi.org/10.1016/j.memsci.2018.09.060.

Yang, J., Li, H.N., Chen, Z.X., He, A., Zhong, Q.Z., Xu, Z.K., 2019. Janus membranes with controllable asymmetric configurations for highly efficient separation of oil-in-water emulsions. J. Mater. Chem. A 7, 7907–7917. https://doi.org/10.1039/C9TA00575G.

Zhang, L., Gu, J.C., Song, L.P., Chen, L., Huang, Y.J., Zhang, J.W., Chen, T., 2016. Underwater superoleophobic carbon nanotubes/core-shell polystyrene@Au nanoparticles composite membrane for flow-through catalytic decomposition and oil/water separation. J. Mater. Chem. A 4, 10810–10815. https://doi.org/10.1039/C6TA04362C.

Zhang, P., Wang, Q., Fang, Y., Chen, W.M., Kirchon, A.A., Baci, M., Feng, M.B., Sharma, V.K., Zhou, H.C., 2016b. Metal-organic frameworks as selectivity regulators for hydrogenation reactions. Nature 539, 203–229. https://doi.org/10.1038/nature19763.

Zhang, Y.Q., Yang, X.B., Wang, Z.X., Long, J., Shao, L., 2017. Designing multifunctional 3D magnetic foam for effective insoluble oil separation and rapid selective dye removal for use in wastewater remediation. J. Mater. Chem. A 5, 7316–7325. https://doi.org/10.1039/C6TA11252H.

Zhang, S.X., Jiang, G.S., Gao, S.J., Jin, H.L., Zhu, Y.Z., Zhang, F., Jin, J., 2018a. Cupric phosphate nanosheets-wrapped inorganic membranes with superhydrophilic and outstanding anticrude oil-fouling property for oil/water separation. ACS Nano 12, 795–803. https://doi.org/10.1021/acsnano.7b08121.

Zhang, X.D., Wang, X.L., Liu, X.H., Lv, C.J., Wang, Y.M., Zheng, G.Q., Liu, H., Liu, C.T., Guo, Z.H., Shen, C.Y., 2018b. Porous polyethylene bundles with enhanced hydrophobicity and pumping oil-recovery ability via skin-peeling. ACS Sustain. Chem. Eng. 6, 12580–12585. https://doi.org/10.1021/acssuschemeng.8b03305.

Zhang, X.D., Pan, Y.M., Gao, Q.S., Zhao, J.Y., Wang, Y.M., Liu, C.T., Shen, C.Y., Liu, X.H., 2019a. Facile fabrication of durable superhydrophobic mesh via candle soot for oil water separation. Prog. Org.Coat. 136, 105253. https://doi.org/10.1016/j.porgcoat.2019.105253.

Zhang, Z.J., Yang, Y., Lia, C.L., Liu, R., 2019b. Porous nanofibrous superhydrophobic membrane with embedded Au nanoparticles for the integration of oil/water separation and catalytic degradation. J. Membrane Sci. 582, 350–357. https://doi.org/10.1016/j.memsci.2019.04.024.

Zhang, M.C., Mao, Y.Y., Liu, G.Z., Liu, G.P., Fan, Y.Q., Jin, W.Q., 2020. Molecular bridges stabilize graphene oxide membranes in water. Angew. Chem. Int. Ed. 59, 1689–1695. https://doi.org/10.1002/anie.201913010.

Zhu, Q., Pan, Q.M., 2014. Mussel-inspired direct immobilization of nanoparticles and application for oil-water separation. ACS Nano 2, 1402–1409. https://doi.org/10.1021/nn4052277.